Precision Engineering 37 (2013) 483–490

Contents lists available at SciVerse ScienceDirect

Precision Engineering

journal homepage: www.elsevier.com/locate/precision

Semi-empirical material removal rate distribution model for SiO_2 chemical mechanical polishing (CMP) processes

H.S. Lee [a,*], H.D. Jeong [a], D.A. Dornfeld [b]

[a] School of Mechanical Engineering, Pusan National University 30, Jangjeon-dong, Geumjeong-gu, Busan 609-735, Republic of Korea
[b] Department of Mechanical Engineering, University of California, Berkeley, CA 94720-1740, USA

ARTICLE INFO

Article history:
Received 24 August 2012
Received in revised form
20 December 2012
Accepted 28 December 2012
Available online 10 January 2013

Keywords:
Chemical mechanical polishing (CMP)
Material removal rate (MRR)
MRR distribution
Modeling

ABSTRACT

A novel semi-empirical model was developed for predicting the material removal rate (MRR) during chemical mechanical polishing (CMP) based on the following assumptions: plastic contact at the wafer–particle interface, elastic contact at the pad–particle interface, a particle size distribution, and a randomly distributed surface roughness of the polishing pad. The proposed model incorporates the effects of particle size, concentration, and distribution, as well as the slurry flow rate, pad surface topography, material properties, and chemical reactions during the silicon dioxide (SiO_2) CMP. To obtain the unknown parameters and ensure the validity of the model, a SiO_2 CMP experiment was conducted by using various-sized CMP slurries. The spatial distribution of the MRRs is expressed with respect to the normal contact stress distribution and the relative velocity distribution. The proposed MRR model can be used for the development of a CMP simulator, the optimization of CMP process parameters, and the design of next-generation CMP machines.

1. Introduction

Chemical mechanical polishing (CMP) is a process of smoothing and planarizing wafer surfaces by using a combination of chemical reactions and mechanical forces [1]. Numerous parameters are involved in the material removal process, such as the type of abrasive, pressure on the wafer, relative velocity between the polishing pad and the wafer, slurry chemistry, polishing pad, and substrate characteristics [2–5]. The modeling of the material removal rate (MRR) is crucial to understand the complexity of the CMP process, and considerable research efforts have been concentrated on this topic. The fundamentals of silicon dioxide (SiO_2) CMP are understood via studies of glass polishing. The predominant mechanism responsible for SiO_2 removal is the mechanical abrasion followed by the hydration of the SiO_2 surface in the presence of an alkaline slurry [6,7]. The hydrated layer is rapidly formed on the SiO_2 surface by the indentation of the silica particles against the SiO_2 film in the slurry [8].

Early models of CMP were based on glass polishing technology and the MRR was described by Preston's equation [9], which indicates that the product of the pressure and the relative velocity between the wafer and the polishing pad contributes significantly toward the MRR. Alternatively, Runnels and Eyman [10] replaced the applied pressure and the relative velocity with normal and tangential stresses at the wafer–pad interface in Preston's equation. In addition, Liu et al. [11] developed a CMP model based on elastic theory and the kinematics of an abrasive particle moving in the gap of a pair of surfaces in rolling contact. Fu et al. [12] assumed that perfect plastic deformation occurred when particles abraded the softer hydrated layer on the SiO_2 surface. Luo and Dornfeld [13] investigated the material removal model under the following assumptions: plastic contact between the wafer–abrasive and the pad–abrasive interfaces, a periodic roughness of the polishing pad, and a normal distribution of particle size. The synergetic effect of chemical and mechanical forces was represented by a dynamic hardness of the wafer surface. Zhao and Chang [14] proposed a CMP model for silicon wafer based on contact mechanics. In their model, plastic contact at the wafer–particle interface and elastic contact at the particle–pad interface were assumed for calculating the indentation depth of the particle in the wafer surface. The line density of uniformly dispersed particles in the slurry and the real contact area between the wafer and the polishing pad were used to calculate the number of active particles. Qin et al. [15] took into account the chemical and mechanical interactions involved in a typical CMP process, using the thickness of the thin chemically modified layer and the indentation depth of the particle into the wafer surface to understand the nonlinear behavior of the MRR. Lin [16] described the relationship between the polishing parameters and the MRR with an analytical model on the basis of elastic and elastic–plastic deformations during a polishing process. Jiang et al. [17] modified

* Corresponding author. Tel.: +82 51 510 3210; fax: +82 51 518 8442.
E-mail address: hyunseop.lee@pusan.ac.kr (H.S. Lee).

0141-6359/$ – see front matter © 2013 Elsevier Inc. All rights reserved.
http://dx.doi.org/10.1016/j.precisioneng.2012.12.006

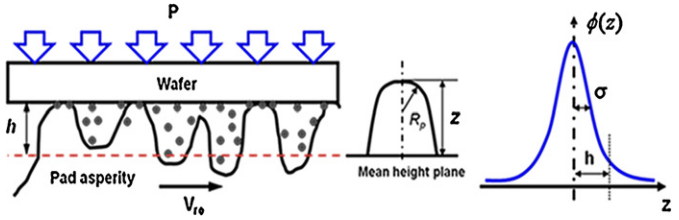

Fig. 1. Schematic of the pad surface topology in contact with the chemically modified layer on the wafer surface and the distribution of the pad asperity heights (P is the pressure; h is the height of the asperity; V_{re} is the relative velocity; R_p is the average radius of curvature of the tip of the pad asperity; and φ is the normal distribution function.) [15].

Zhao and Chang's model to understand the removal of the amorphous layer on the wafer surface by a single particle based on the viscous flow of the amorphous layer.

The MRR distribution in SiO_2 CMP is determined by the distributions of relative velocity and normal stress between the wafer and the polishing pad [18]. Hocheng et al. [19] proposed a model for material removal using abrasive cutting, which provided a part of the analytical background for the empirical Preston's equation. The uniformity of the relative velocity between the wafer and the pad at any point was determined by a kinematic analysis. Kim and Jeong [20] calculated the velocity distribution, sliding distance of the wafer, and sliding distance of the polishing pad in order to verify the effect of the process conditions on the velocity uniformity and the wear distance of the pad and the wafer.

Researchers studying the MRR distribution in CMP have focused on the stress distribution caused by the applied pressure of the carrier by using a finite element analysis (FEA) method or a mathematical analysis. Wang et al. [21] introduced the concept of a Von Mises stress in the analysis of the MRR distribution by using commercial FEA software. Subsequently, many researchers began applying a Von Mises stress in the analysis of CMP processes. Srinivasa-Murthy et al. [22] investigated the variations in the Von Mises stress on the wafer surface using a 3D model in rectangular Cartesian coordinates. Chen et al. [23] utilized the normal contact stress as a stress indicator in CMP and concluded that the Von Mises and normal contact stresses are not equivalent, which is a significant finding. The normal contact stress is an appropriate stress index because the frictional force is proportional to the normal contact stress. Lee and Jeong [24] integrated the effects of the normal contact stress, relative velocity, and chemical reaction rate distributions of Cu CMP by an empirically obtained spatial parameter.

However, there is still room for a better theoretical understanding of removal mechanisms for modeling the CMP process, because the MRR models and the MRR distribution models have been studied independently. In this paper, we propose an integrated MRR distribution model that incorporates the effects of the material properties of the particles, wafer, and polishing pad, and process conditions such as pressure, relative velocity, and slurry flow rate.

2. Model development

2.1. Real contact area and contact pressure

Fig. 1 shows the pad surface topology in contact with the chemically modified layer on the wafer surface and the distribution of the pad asperity heights. The polishing pad is made of porous urethane. The distribution of the pad asperity height follows the normal distribution function. The roughness of the wafer surface is small; compared to the pad, the wafer surface is assumed to be a smooth plane.

Based on the Greenwood–Williamson model [25] and contact mechanics [26], Qin et al. [15] reported that the real contact area (A_r) for CMP between a smooth, flat wafer and a randomly rough pad under a normal force (F) can be expressed as

$$A_r = \left(\frac{f_s}{C}\right)\left(\frac{R_p}{\sigma_p}\right)^{1/2}\frac{PA_w}{E_{pw}}, \tag{1}$$

where σ_p is the standard deviation of the pad asperity height (z) distribution; f_s is the area density of the up-features divided by the area of a flat pad; R_p is the average radius of curvature of the pad asperity tips; and $E_{pw}(E_{pw} = ((1-\nu_p^2)/E_p + (1-\nu_w^2)/E_w)^{-1})$ is the composite Young's modulus of the pad and the wafer. In a CMP process, C is a constant with a value between 0.3 and 0.4 when h/σ_p is in the range of 0.5–3.0 [15]. C can be taken as approximately 0.35 because any practical situation in a typical CMP process is within this h/σ_p range [15].

The contact pressure (P_r) can be calculated as

$$P_r = \left(\frac{C}{f_s}\right)\left(\frac{\sigma_p}{R_p}\right)^{1/2}E_{pw}, \tag{2}$$

where P is the applied pressure and A_w is the nominal area of the wafer surface.

The contact pressure does not depend on the normal force. Instead, the real contact area increases linearly with increasing normal force because it is assumed that the applied load is supported by the pad asperities at the wafer–asperity contact surface. The hydrodynamic pressure is negligible because commercial pads have grooves or perforations to prevent hydroplaning and ensure uniform slurry distribution [15]. The area density of the up-features divided by the area of a flat pad, f_s ($0 < f_s \leq 1$), was reported to be 0.83 for an IC1000 (k-groove) pad [27].

2.2. Number of active particles

Previous research on calculating the number of active particles in CMP has not considered the slurry flow rate because the active particles were only calculated from the volume concentration of the particles in the slurry [14–17]. If we consider the previously reported line density of particles given by Ref. [14], we see that the MRR becomes independent of the size of the particles. In order to overcome these analytical shortcomings, we obtained a line density from an imaginary slurry volume on the apparent wafer–pad sliding area (A_w^T), which was calculated from the total contact area between the rotating wafer and the polishing pad during the process.

Earlier studies indicate that the size distribution of the particles satisfies a probability density function ($\Phi(D)$) [14]. All of the particles are spherical in shape and estimated to be uniformly dispersed in the slurry. We assumed that the particles are rearranged in the imaginary slurry volume in the apparent wafer–pad sliding area as they participate in the polishing and that the particles embedded in the polishing pad participate in the material removal process.

The weight of a single particle ($\omega(D)$) can be calculated as

$$\omega(D) = \frac{1}{6}\pi D^3\rho_a, \tag{3}$$

where D is the diameter of a particle and ρ_a is its density.

The total number of particles in the slurry container can be written as

$$N_p = \frac{X\rho_s C_a}{\int_0^{+\infty}\Phi(D)\omega(D)dD}, \tag{4}$$

where ρ_s is the density of the slurry; C_a is the weight concentration of the particle; $\Phi(D)$ is the probability density function; and X is the total slurry volume during CMP.

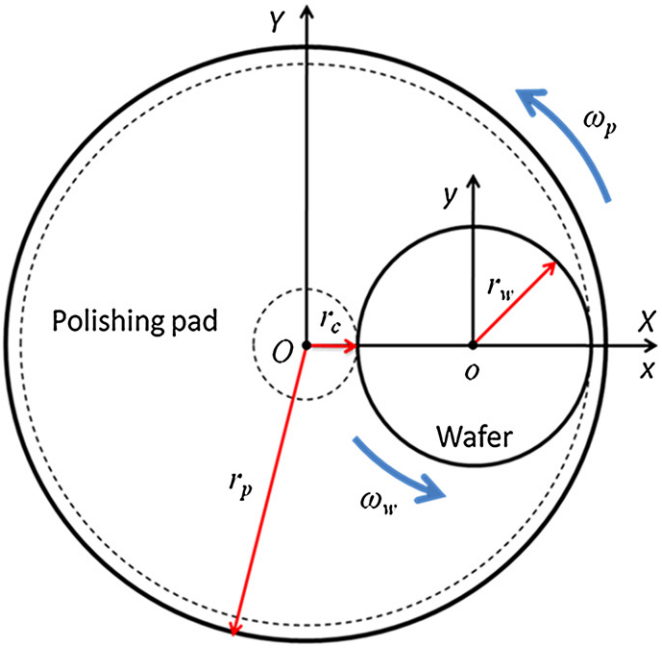

Fig. 2. Schematic diagram of kinematic system of the CMP process.

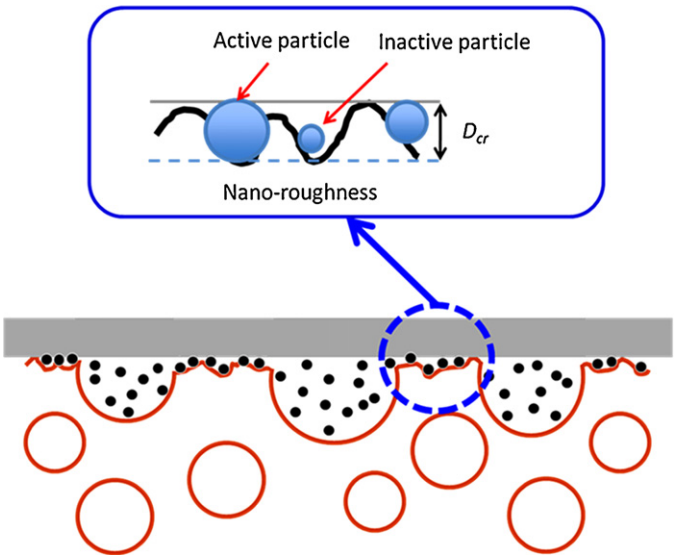

Fig. 3. Schematic of active particles and the critical diameter (D_{cr}).

The apparent wafer–pad sliding area is calculated as

$$A_w^T = \pi n_p[(r_c + 2r_w)^2 - r_c^2] \tag{5}$$

where n_p is the number revolutions of the polishing pad; r_c is the length between the center of the polishing pad and the inner boundary of the wafer sliding area; and r_w is the radius of the wafer, as shown in Fig. 2.

The imaginary slurry thickness (t_s) in the apparent wafer–pad sliding area can be obtained from Eq. (6).

$$t_s = \frac{X}{A_w^T} \tag{6}$$

The distance (l) between rearranged particles in the hypothetical slurry volume that contains N_p particles can be obtained by solving

$$l^3 - \left(\frac{2\sqrt{A_w^T} + t_s}{N_p - 1}\right) \cdot l^2 - \left(\frac{2\sqrt{A_w^T}t_s + A_w^T}{N_p - 1}\right) \cdot l - \left(\frac{A_w^T t_s}{N_p - 1}\right) = 0. \tag{7}$$

The area density of particles (q) can be obtained from the distance between particles:

$$q = \frac{\left(\sqrt{A_w^T}/l + 1\right)^2}{A_w^T}. \tag{8}$$

The particles in the CMP slurry are statistically distributed and have a mean diameter with a standard deviation. Because some of the particle sizes are much smaller than the nano-scale roughness of the polishing pad, not all of the particles participate in the material removal process. In this paper, the abrasive particles that are involved in the removal process are called active particles. They have a diameter that is greater than the critical particle diameter (D_{cr}), as shown in Fig. 3 [28]. Therefore, the total number of active particles (n_a) that participate in material removal during CMP is expressed as

$$n_a = qA_r \int_{D_{cr}}^{+\infty} \Phi(D)dD = \frac{\left(\sqrt{A_w^T}/l + 1\right)^2}{A_w^T} \times \left(\frac{f_s}{C}\right)\left(\frac{R_p}{\sigma_p}\right)^{1/2} \frac{PA_w}{E_{pw}} \int_{D_{cr}}^{+\infty} \Phi(D)dD, \tag{9}$$

where D_{cr} is the critical particle diameter of particles that can participate in the material removal process.

2.3. Calculation of average MRR

Because the pad material is much softer than the wafer material, the particles at the wafer–pad interface are located on the contact asperities of the pad surface after the wafer presses on the polishing pad. The down-force is sustained by the contact asperities and embedded particles in the pad surface. With respect to particle indentation, the polishing pad and the wafer experience different modes of deformation because they have different mechanical properties. Zhao and Chang [14] reported that the particle indentation deformation associated with the pad is elastic and the deformation associated with the wafer is fully plastic. Wang et al. [29] proposed an equation for the indentation depth of a single particle into the pad surface by using a parabolic approximation for the profile of a sphere. In this study, we adopted Wang's nonlinear and micro-contact model for a single particle and incorporated large elastic pad deformation from the particle–pad contact. Additionally, according to Zhao and Chang's research, we assumed that there is plastic deformation at the wafer–particle interface and elastic deformation at the pad–particle interface.

The indentation depth of the particle in the wafer–particle–pad system is determined based on the force equilibrium of the particle participating in the wear process. Fig. 4 shows the wafer–particle–pad micro-contact. The parabolic approximation of the profile of the spherical particle (diameter, D) [29] is

$$f(x) = \frac{D}{2} - \sqrt{\left(\frac{D}{2}\right)^2 - (ax)^2} \quad \text{and} \quad x = \frac{r}{a}. \tag{10}$$

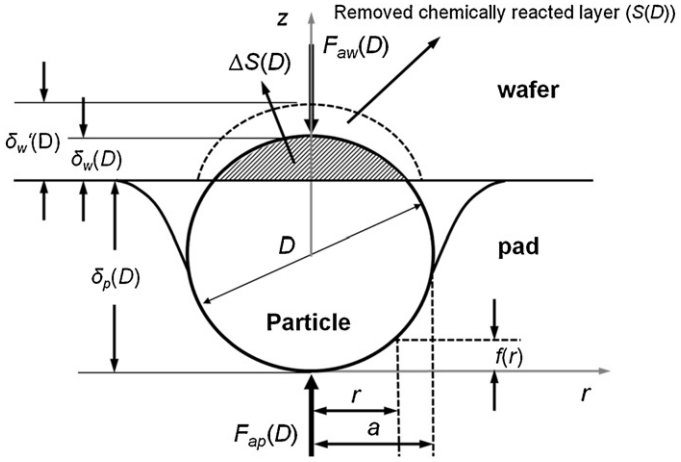

Fig. 4. Schematic of pad–wafer–particle contact [29].

The indentation depth of the particle into the pad is [26]

$$\delta_p(D) = \int_0^1 \frac{f'(x)}{\sqrt{1-x^2}}dx. \tag{11}$$

The force equilibrium ($F_{aw}(D) = F_{ap}(D)$) of the plastic contact between the particle and the wafer (F_{aw}) and the elastic contact between the pad and the particle (F_{ap}) with a boundary condition on the indentation depth ($F_{aw}(D) = H_{w\pi}D_{\delta w}(D)$) allows the indentation depth of a particle into the wafer surface to be calculated by solving [29]

$$\left(\frac{H_w}{E_{ap}}\right)^2 = \frac{1}{8\pi^2}\frac{(2\zeta+(\zeta-1)(-3+\sqrt{9+12\zeta}))^2}{(2-\zeta)^2(-3+\sqrt{9+12\zeta})}, \tag{12}$$

where

$$\zeta = \frac{2\delta_p(D)}{D}.$$

The indentation depth of a particle into the wafer ($\delta_w(D)$) [29] is defined as

$$\delta_w(D) = \left(1-\frac{\zeta}{2}\right)D. \tag{13}$$

In Eqs. (10)–(13), $\delta_p(D)$ is the indentation depth of the particle of diameter D in the polishing pad, H_w is the hardness of the film to be removed, $\delta_w(D)$ is the indentation depth of the particle of diameter D into the wafer surface, and E_{ap} is the composite Young's modulus of the pad and particle.

After the slurry chemicals change the material properties of the wafer surface, the chemically reacted surface layer can be removed by the mechanical action of the abrasive particles. Assuming that the reacted surface layer is thick enough, the indentation of the particles into the wafer surface causes plastic deformation in the reacted surface layer. The chemically reacted surface is softer than the original surface and is more readily removed by the sliding particles. In Fig. 4, $\Delta S(D)$ is the cross-sectional removal area calculated from the indentation depth of a single particle of diameter D for the original surface and $S(D)$ is the cross-sectional removal area for the chemically reacted surface. $\delta_w(D)$ is the equivalent indentation depth of a single particle of diameter D for the original surface and $\delta'_w(D)$ is the equivalent indentation depth for the chemically reacted surface. To calculate the real MRR, it is assumed that $S(D)$ is proportional to $\Delta S(D)$ and the proportional constant is obtained from the comparison of the model and the experimental data. $S(D)$ is expressed as

$$S(D) = k\Delta S(D) = \frac{4}{3}k\delta_w(D)\sqrt{\delta_w(D)D}. \tag{14}$$

Based on the number of active particles and the particle indentation, the average MRR (MRR_{avg}) is expressed as follows:

$$MRR_{avg} = \left(\frac{4}{3}k\frac{\left(\sqrt{A_w^T}/l+1\right)^2}{A_w^T}\left(\frac{f_s}{C}\right)\left(\frac{R_p}{\sigma_p}\right)^{1/2}\frac{PV_{re.avg}}{E_{pw}}\left(1-\frac{\zeta}{2}\right)^{3/2}\right) \cdot \int_{D_{cr}}^{+\infty}\Phi(D)D^2dD, \tag{15}$$

where k is a constant obtained from the experimental data and $V_{re.avg}$ is the average relative velocity of the wafer.

The equivalent indentation depth of a single particle can be calculated from the experimentally obtained k value, as shown below:

$$\delta'_w(D) = k^{2/3}\delta_w(D) = \left(1-\frac{\zeta}{2}\right)k^{2/3}D. \tag{16}$$

Therefore, the average MRR in Eq. (15) is rewritten with the equivalent indentation depth as follows:

$$MRR_{avg} = \left(\frac{4}{3}\frac{\left(\sqrt{A_w^T}/l=1\right)^2}{A_w^T}\left(\frac{f_s}{C}\right)\left(\frac{R_p}{\sigma_p}\right)^{1/2}\frac{PV_{re.avg}}{E_{pw}}\left(1-\frac{\zeta'}{2}\right)^{3/2}\right) \cdot \int_{D_{cr}}^{+\infty}\Phi(D)D^2dD, \tag{17}$$

where

$$\zeta' = 2-k^{2/3}(2-\zeta).$$

2.4. MRR distribution model

The spatial distribution of the MRR can be expressed by using a spatial parameter consisting of the normalized normal contact stress and the normalized average relative velocity distribution, as shown below: [24]

$$MRR(x,y) = MRR_{avg}\cdot\left\{\left(\frac{\sigma_n(x,y)}{\sigma_{n.avg}}\right)^{\alpha}\left(\frac{V_{re.avg}(x,y)}{V_{re.avg}}\right)^{\beta}\right\}, \tag{18}$$

where $\sigma_n(x,y)$ is the normal contact stress at an arbitrary position on the wafer; $\sigma_{n.avg}$ is the average normal contact stress; $V_{re.avg}(x,y)$ is the average relative velocity at an arbitrary position on the wafer; and $V_{re.avg}$ is the average relative velocity of the wafer. The normal contact stress distribution can be obtained from an FEA simulation and the relative velocity distribution can be calculated using a kinematic analysis that accounts for the operating conditions. However, it is inappropriate to compare the influence of each parameter on the MRR distribution because the units and magnitudes of the normal contact stress and the relative velocity are different. All of the parameters are normalized with respect to their average values to represent their deviations; α and β are constants that represent the influence of each normalized parameter. When the angular velocity of the carrier equals that of the platen, the value of $V_{re.avg}(x,y)/V_{re.avg}$ is "1" and the MRR distribution depends only on the normalized normal contact stress. In this study, we only considered the normal contact stress distribution by setting the angular velocities of the carrier and the platen equal to each other.

Table 1
CMP slurries for experiments.

Slurry	Mean (nm)	Standard deviation (nm)
D13	13.3	3.7
D22	22.4	4.4
D61	60.9	12.5
D118	117.7	26.4

3. Experimental conditions

An IC1000/SubaIV stacked pad (Nitta Haas Inc., Japan) was used as the stacked form, composed of an IC1000 (polyurethane pad) as the top pad and a SubaIV (felt-type pad) as the base, and it was designed for easy use and for improving the performance consistency. A plasma-enhanced chemical vapor deposition (PECVD) was used to deposit a silicon dioxide (SiO_2) film (1.5 μm thick) on an 8-in. (200 mm) silicon wafer. The CMP process was performed using a rotary CMP polisher (GnP POLI500, GnP Technology, Korea). The distance from the center of the platen to the center of the carrier was 130 mm. The carrier was estimated to be devoid of oscillations during the CMP process. The operating pressures were 27.58 kPa for the wafer and 34.47 kPa for the retaining ring. The relative velocity was 65.312 m/min, and the slurry flow rate was 150 ml/min. Four-types of CMP slurries were prepared for the experiments, as shown in Table 1. The particle diameter was measured with a particle-size analyzer (ELS-8000, OTSUKA Electronics Co.). The mean particle diameters for the four slurries were 13.3 nm (D13), 22.4 nm (D22), 60.9 nm (D61), and 117.7 nm (D118). The concentration of particles was fixed at 12.5 wt%. During CMP, the conditioning process was ex situ at a pressure of 5.88 kPa and rotational velocities of 40 rpm for the conditioner disk and 60 rpm for the platen. After polishing for 1 min, the thickness of the SiO_2 films was measured using a reflectometer (K-Mac ST5030-SL). The MRRs of the SiO_2 films were measured at 41 points on each wafer, and the edge exclusion was 3 mm.

4. Experimental verification and discussion

Park and Jeong [30] reported the real contact area ratio (real contact area/nominal contact area) without considering the grooves of the polishing pad before and after conditioning. When the applied pressure was 34.47 kPa, the real contact area ratio of the as-received polishing pad was 0.0027, and the real contact area ratios after a conditioning process with a random diamond disk (RDD) and a uniform diamond disk (UDD) were 0.0089 and 0.0145, respectively. Considering the area density of the up-features divided by the area of a flat pad (f_s: 0.83), the real contact area ratios at 5 psi were calculated to be 0.0074 and 0.0120 for the RDD and the UDD, respectively. These values of the real contact area are similar to the experimentally reported range. According to Eq. (1) and the material properties in Table 2, the real contact area ratio in this study

Table 2
Material properties for CMP modeling.

Variable	Description	Value	Unit
σ_p	Standard deviation of pad asperity	30	μm
R_p	Average radius of pad asperity	25	μm
E_p	Young's modulus of pad material	10	MPa
υ_p	Poisson ratio of pad material	0.2	–
E_a	Young's modulus of silica particle	94	GPa
υ_a	Poisson ratio of silica particle	0.26	–
ρ_a	Density of silica particle	2270	kg/m^3
ρ_s	Density of slurry	1040	kg/m^3
E_w	Young's modulus of silicon dioxide	66	GPa
υ_w	Poisson ratio of silicon dioxide	0.3	–
H_w	Hardness of silicon dioxide	18	GPa

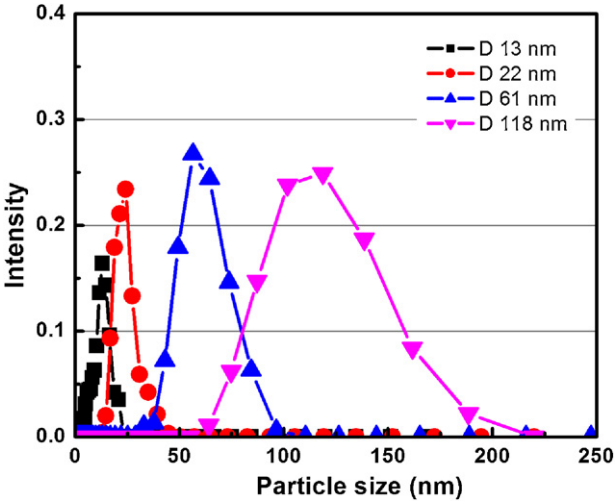

Fig. 5. Particle size distributions of slurries.

at 34.47 kPa is 0.0086. For a pressure of 27.58 kPa, the real contact area ratio is calculated to be 0.0052.

For the model, D_{cr} is assumed to be 22 nm. The MRR at a particle diameter of 118 nm was used to calculate the value of k, and k was obtained from the comparison between the model and the experimental data to be 1.21. The size distribution of the particles is measured as a discrete probability density distribution, as shown in Fig. 5. The discrete probability density function is used to calculate the total number of particles.

The value of k indicates that the SiO_2 surface is softened by the chemical reaction with the slurry because the chemicals in a CMP slurry change the mechanical properties of the wafer surface. This chemically reacted surface layer is then removed by the abrasive mechanical action of the sliding particles in the slurry. If the chemically reacted surface layer is thick enough, the indentation of the particles into the wafer causes plastic deformation of the reacted layer. According to Sorooshian et al. [31], the etch rate of SiO_2 in the oxide slurry is approximately zero. The predominant phenomenon responsible for the removal of SiO_2 is a combination of chemical and mechanical interactions that first hydrate the SiO_2 surface owing to the presence of the alkaline slurry and then mechanically abrade the surface with the particles present in the slurry. In SiO_2 CMP, material removal by chemical etching is negligible for the modeling of MRR.

Fig. 6 shows the experimentally obtained average MRRs and the calculated average MRRs as a function of particle diameter, with the

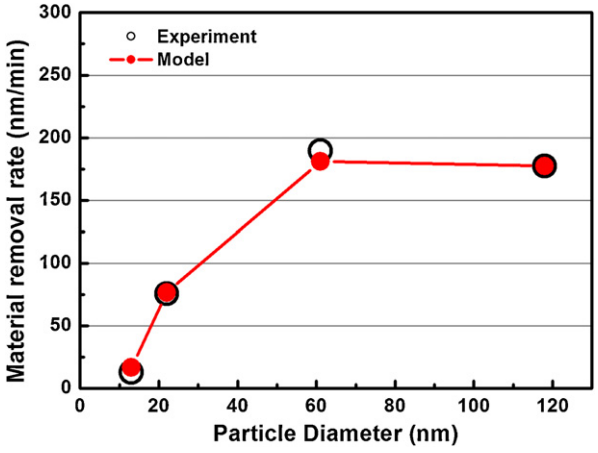

Fig. 6. Average MRR as a function of average particle size.

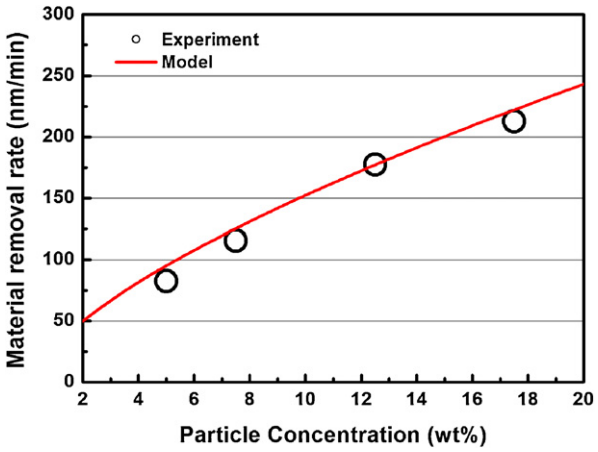

Fig. 7. Average MRR as a function of particle concentration (D118).

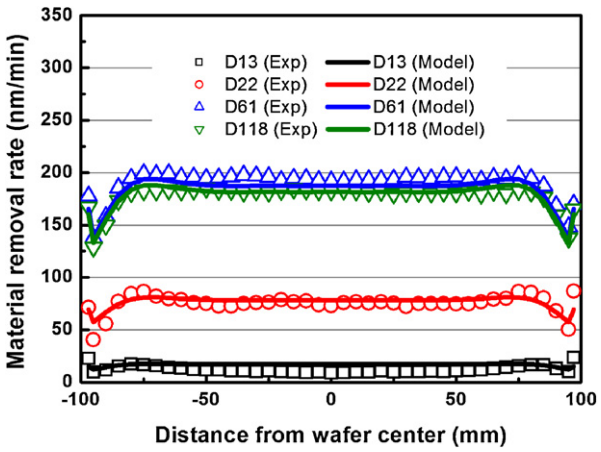

Fig. 8. Experimental and calculated MRR distributions for various particle diameters (C_a: 0.125).

particle concentration fixed at 12.5 wt%. The MRR increases from D13 to D61, and decreases slightly from D61 to D118. Zhou et al. [32] obtained similar results in the CMP of a SiO_2 film using six kinds of colloidal silica slurries with different mean particle diameters of 10, 20, 50, 80, 110, and 140 nm. They found that the 80 nm silica particle exhibited the highest MRR and best surface finish. Zhang et al. [33] also reported a similar experimental result on the effect of the mean particle size on the MRR. As is seen in Fig. 6, the MRRs predicted by the model are in agreement with the experimentally measured MRRs under the same CMP conditions.

Fig. 7 shows the experimentally measured average MRRs and the predicted average MRRs from Eq. (15) as a function of particle concentration for the D118 slurry. The particle concentration was varied from 5 wt% to 17.5 wt%. Mahajan's experiment [34] showed a similar trend for SiO_2 CMP with 0.2 μm silica particles. The MRR increases with the particle concentration, indicating that the presence of more active particles increases the material removal of SiO_2. However, Choi et al. [35] showed that the increase in particle concentration leads to an increased MRR for low particle concentrations; conversely, for high particle concentrations, the MRR decreases with increasing particle concentration. However, they used 0.2, 0.5, 1.0, and 1.5 μm particles, which are larger than the particles used for this study. They explained their experimental results via the dynamic motion of silica particles: sliding motion for low particle concentrations and rolling motion for high particle concentrations. Only the CMP results using 0.2 μm particles show a similar trend to our experimental data and modeling results. Our model cannot predict the effects of rolling motion because we assumed that the SiO_2 film is removed by a two-body abrasion caused by the sliding motion of the imbedded particles in the pad surface. However, the typical particle size in CMP is less than 200 nm [2,36], and the size distribution is tightly controlled to prevent particle agglomeration that results in scratches. Zhou et al. [32] concluded that for SiO_2 CMP, the MRR increases with the increase in particle concentration for the nano-scale abrasives, which is different than the trend for micro-scale abrasives. Therefore, the proposed model is plausible for explaining the MRR for SiO_2 CMP processes involving nano-scale abrasives.

Normal contact stress uniformity is a key parameter in wafer-level CMP performance because it relates to the frictional force. In this study, the normal contact stress distribution in the CMP process is considered with a 2D axisymmetric model. The CMP finite element model consists of a polishing pad, wafer, and carrier film. The pressure on the back of the carrier is assumed to be uniformly distributed. The following assumptions are also made: all the materials are isotropic and homogeneous; the surfaces of the backing film, wafer, retainer ring, PC film, and pad are smooth; the wafer and the polishing pad are in contact at every point of the interface at which small sliding occurs; and the relative velocity between the wafer and the polishing pad is constant at all positions. For the model, a quadrilateral mesh was used, and the numbers of nodes and elements were 115,496 and 34,780, respectively. Because the rotational velocity of the carrier is equivalent to that of the platen, the relative velocity distribution does not influence the theoretical MRR distribution.

Figs. 8 and 9 show the distributions of the measured and predicted MRRs. Specifically, Fig. 8 shows the measured and predicted results of the model using various particle diameters with a concentration of 12.5 wt%. Fig. 9 shows the experimental and calculated MRR distributions of the D118 slurry for various particle concentrations. α was calculated to be 3.77 from the comparison between the experimental data and the proposed model. The constant in the regression is negligible. The average normalized MRRs of each measuring point in the experiments on particle size effect were compared with the normalized stress distribution because the particle concentration may largely impacts MRRs near the edge of the wafer. Both outermost measuring points were ignored because of the irregularity. The correlation coefficient was 0.818 and the stress distribution positively correlated with the MRR distribution. Table 3 shows the normalized stress distribution and the average normalized MRR for regression analysis. The distribution of the MRRs follows the distribution of the normal contact stress. The results show that the MRRs are distributed uniformly at the center

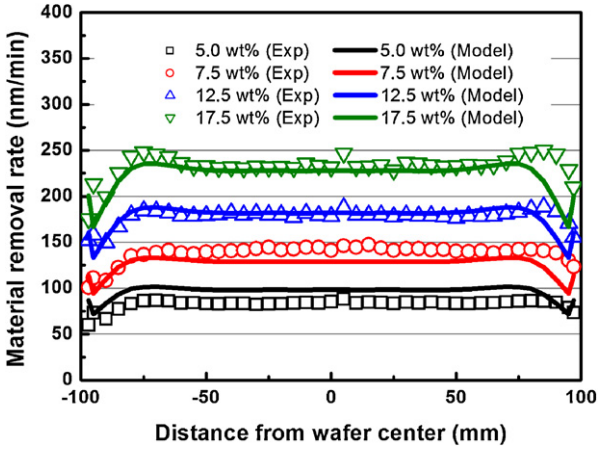

Fig. 9. Experimental and calculated MRR distributions for various particle concentrations (D118).

Table 3
Normalized stress distribution and average normalized MRR for regression analysis.

Position	Normalized stress	Avg. normalized MRR
−95	0.9268	0.6835
−90	0.9644	0.8342
−85	0.9932	1.0449
−80	1.0092	1.1298
−75	1.0152	1.1316
−70	1.0155	1.0962
−65	1.0134	1.0584
−60	1.0109	1.0334
−55	1.0089	1.0065
−50	1.0074	0.9957
−45	1.0065	0.9821
−40	1.0062	0.9697
−35	1.0062	0.9780
−30	1.0065	0.9684
−25	1.0067	0.9763
−20	1.0066	0.9675
−15	1.0063	0.9628
−10	1.0062	0.9554
−5	1.0067	0.9472
0	1.0067	0.9276
5	1.0067	0.9440
10	1.0062	0.9528
15	1.0063	0.9489
20	1.0066	0.9786
25	1.0067	0.9495
30	1.0065	0.9477
35	1.0062	0.9586
40	1.0062	0.9662
45	1.0065	0.9581
50	1.0074	0.9707
55	1.0089	0.9771
60	1.0109	0.9874
65	1.0134	1.0348
70	1.0155	1.0518
75	1.0152	1.1089
80	1.0092	1.1215
85	0.9932	1.0872
90	0.9644	0.9261
95	0.9268	0.7506

of the wafer; however, the MRRs near the edge of the wafer reduce and then increase at the outermost radius, according to the normal contact stress distribution. Some errors near the wafer edge may be caused by the slurry flow, which was not considered in the model. Nevertheless, the predicted results and measured results show good agreement.

5. Conclusions

Based on contact mechanics, this paper proposes a MRR model for SiO_2 CMP, incorporating the effects of particle size, particle concentration, slurry flow rate, area density of the pad surface, and chemical reactions. It is assumed that the polishing pad has a randomly rough surface, plastic contact occurs at the wafer–particle interface, and the polishing pad deforms elastically via particle indentation. The proposed model includes the line density of particles from an imaginary slurry volume in the wafer–pad sliding area, which has not been included in previous models. The predicted results show good agreement with the experimentally obtained results. The proposed MRR model can be used for the development of a CMP simulator, the optimization of process parameters, and the design of the next-generation of CMP machines.

Acknowledgments

The authors gratefully acknowledge the support of G&P Technology Inc., Republic of Korea and LMAS at UC Berkeley (http://lma.berkeley.edu).

References

[1] Lee HS, Jeong HD. Chemical and mechanical balance in polishing of electronic materials for defect-free surfaces. CIRP Annals-Manufacturing Technology 2009;58:485–90.
[2] Zantye PB, Kumar A, Sikder AK. Chemical mechanical planarization for microelectronics applications. Materials Science and Engineering R 2004;45:89–220.
[3] Steigerwald JM, Shyam P, Gutmann M, Gutmann RJ. Chemical mechanical planarization of microelectronic materials. New York: Wiley; 1997.
[4] Lee H, Joo S, Jeong H. Mechanical effect of colloidal silica in copper chemical mechanical planarization. Journal of Materials Processing Technology 2009;209:6134–9.
[5] Larsen-Basse J, Liang H. Probable role of abrasion in chemo-mechanical polishing of tungsten. Wear 1999;233-235:647–54.
[6] Cook LM. Chemical process in glass polishing. Journal of Non-Crystalline Solids 1990;120:152–71.
[7] Tomozawa M. Oxide CMP mechanisms. Solid State Technology 1997;40:39–53.
[8] Nogami M, Tomozawa M. Effect of stress on water diffusion in silica glass. Journal of the American Ceramic Society 1984;67:151–4.
[9] Preston FW. The theory and design of plate glass polishing machine. Journal of the Society of Glass Technology 1927;11:214–56.
[10] Runnels SR, Eyman LM. Tribology analysis of chemical mechanical polishing. Journal of the Electrochemical Society 1994;141(6):1698–701.
[11] Liu CW, Dai TT, Tseng WT, Yeh CF. Modeling of the wear mechanism during chemical mechanical polishing. Journal of the Electrochemical Society 1996;143(2):716–21.
[12] Fu G, Chandra A, Guha S, Subhash G. Plasticity-based model of material removal in chemical–mechanical polishing (CMP). IEEE Transactions on Semiconductor Manufacturing 2001;14:406–17.
[13] Luo J, Dornfeld DA. Material removal mechanism in chemical mechanical polishing: theory and modeling. IEEE Transactions on Semiconductor Manufacturing 2001;14:112–33.
[14] Zhao Y, Chang L. A micro-contact and wear model for chemical–mechanical polishing of silicon wafers. Wear 2002;252:220–6.
[15] Qin K, Moudgil B, Park CW. A chemical mechanical polishing model incorporating both the chemical and mechanical effects. Thin Solid Films 2004;446:277–86.
[16] Lin TR. An analytical model of the material removal rate between elastic and elastic–plastic deformation for a polishing process. International Journal of Advanced Manufacturing Technology 2007;32:675–81.
[17] Jiang JZ, Zhao YW, Wang YG, Luo JB. A chemical mechanical polishing model based on the viscous flow of the amorphous layer. Wear 2008;265:992–8.
[18] Castillo-Mejia D, Beaudoin S. A locally relevant Prestonian model for wafer polishing. Journal of the Electrochemical Society 2003;150(2):G96–102.
[19] Hocheng H, Tsai HY, Tsai MS. Effects of kinematic variables on nonuniformity in chemical mechanical planarization. International Journal of Machine Tools and Manufacture 2000;40:1651–69.
[20] Kim H, Jeong H. Effect of process conditions on uniformity of velocity and wear distance of pad and wafer during chemical mechanical planarization. Journal of Electronic Materials 2004;33:53–60.
[21] Wang D, Lee J, Holland K, Bibby T, Beaudoin S, Cale T. Von Mises stress in chemical–mechanical polishing processes. Journal of the Electrochemical Society 1997;144:1121–7.
[22] Srinivasa-Murthy C, Wang D, Beaudoin SP, Bibby T, Holland K, Cale TS. Stress distribution in chemical mechanical polishing. Thin Solid Films 1997;308–309:533–7.
[23] Chen KS, Yeh HM, Yan JL, Chen YT. Finite-element analysis on wafer-level CMP contact stress: reinvestigated issues and the effects of selected process parameters. International Journal of Advanced Manufacturing Technology 2008;42:1118–30.
[24] Lee H, Jeong H. A wafer-scale material removal rate profile model for copper chemical mechanical planarization. International Journal of Machine Tools and Manufacture 2011;51:395–403.
[25] Greenwood JA, Williamson JBP. Contact of nominally flat surfaces. Proceedings of the Royal Society A 1966;95:300–19.
[26] Johnson KL. Contact mechanics. Cambridge: Cambridge University Press; 1985.
[27] Philipossian A, Yeomans DR. The spectral fingerprints and the sounds of chemical mechanical planarization process. Japanese Journal of Applied Physics 2006;45:1553–9.
[28] Zeng T, Sun T. Size effect of nanoparticles in chemical mechanical polishing – a transient model. IEEE Transactions on Semiconductor Manufacturing 2005;18:655–63.
[29] Wang Y, Zhao YW, Gu J. A new nonlinear-micro-contact model for single particle in the chemical mechanical polishing with soft pad. Journal of Materials Processing Technology 2007;183:374–9.
[30] Park K, Jeong H. Investigation of pad surface topography distribution for material removal uniformity in CMP process. Journal of the Electrochemical Society 2008;155(8):H595–602.
[31] Sorooshian J, DeNardis D, Charns L, Li Z, Shadman F, Boning D, Hetherington D, Philipossian A. Arrhenius characteristic of ILD and copper CMP processes. Journal of the Electrochemical Society 2004;151:G85–8.
[32] Zhou C, Shan L, Hight JR, Danyluk S, Ng SH, Paszkowski AJ. Influence of removal colloidal rate and abrasive size on material surface finish in SiO_2 chemical mechanical polishing. Tribology Transactions 2002;45:232–8.

[33] Zhang Z, Liu W, Song Z. Particle size and surfactant effects on chemical mechanical polishing of glass using silica-based slurry. Applied Optics 2010;49: 5480–5.
[34] Mahajan UD. Fundamental studies on silicon dioxide chemical mechanical polishing. PhD Thesis, Graduate School of the University of Florida; 2000.
[35] Choi W, Abiade J, Lee SM, Singh RK. Effects of slurry particles on silicon dioxide CMP. Journal of the Electrochemical Society 2004;151(8):G512–22.
[36] Haba S, Fukuda K, Ohta Y, Koubuchi Y, Katouda T. Fumed silica slurry stabilizing methods for chemical mechanical polishing. Japanese Journal of Applied Physics 2003;42:418–23.